Quantum capacitance measurements of electron-hole asymmetry and next-nearest-neighbor hopping in graphene

A. Kretinin,[1] G. L. Yu,[2] R. Jalil,[1] Y. Cao,[1] F. Withers,[2] A. Mishchenko,[2] M. I. Katsnelson,[3] K. S. Novoselov,[2] A. K. Geim,[1,2] and F. Guinea[4,5]

[1]*Manchester Centre for Mesoscience and Nanotechnology, University of Manchester, Oxford Road, Manchester, M13 9PL, United Kingdom*
[2]*School of Physics and Astronomy, University of Manchester, Oxford Road, Manchester, M13 9PL, United Kingdom*
[3]*Theory of Condensed Matter, Institute for Molecules and Materials, Radboud University Nijmegen, Heyendaalseweg 135,*
6525 AJ Nijmegen, The Netherlands
[4]*Instituto de Ciencia de Materiales de Madrid (ICMM-CSIC), Cantoblanco, 28049 Madrid, Spain*
[5]*Donostia International Physics Center (DIPC), P. de Manuel Lardizabal 4, 20018, San Sebastián, Basque Country, Spain*

The next-nearest-neighbor hopping term t' determines a magnitude, and, hence, the importance of several phenomena in graphene that include self-doping due to broken bonds and the Klein tunneling, which in the presence of t', is no longer perfect. Theoretical estimates for t' vary widely, whereas a few existing measurements by using polarization-resolved magnetospectroscopy have found surprisingly large t', close to or even exceeding the highest theoretical values. Here, we report dedicated measurements of the density of states in graphene by using high-quality capacitance devices. The density of states exhibits a pronounced electron-hole asymmetry that increases linearly with energy. This behavior yields $t' \approx -0.3$ eV $\pm 15\%$, in agreement with the high end of theory estimates. We discuss the role of electron-electron interactions in determining t' and overview phenomena, which can be influenced by such a large value of t'.

PACS number(s): 72.80.Vp

The conduction and valence bands of graphene are well described by a tight-binding model based on the carbon p_z orbitals. The nearest-neighbor term, $t \approx 3$ eV gives a reasonable description of the Dirac cones at low energies,[1] with a Fermi velocity $v_F = (3ta)/(2\hbar)$, where $a \approx 1.4$ Å is the distance between nearest-neighbor carbon atoms. The bands calculated by assuming only the nearest-neighbor hopping are electron-hole (e-h) symmetric. By also including next-nearest-neighbor hopping, the Hamiltonian and the dispersion relation near the Dirac energy are

$$H = t \sum_{i,j \in n.n.} c_i^+ c_j + t' \sum_{i,j \in n.n.n.} c_i^+ c_j + \text{h.c.}$$

$$\epsilon_{\vec{k}} \approx -3t' \pm \hbar v_F |\vec{k}| + \frac{9}{4} t' |\vec{k}|^2 a^2 + \cdots \quad (1)$$

The position of the Dirac point is shifted by $-3t'$. The breakdown of e-h symmetry does not significantly change the electronic properties of the system at long wavelengths. However, the asymmetry results in a finite dispersion of edge states and changes the midgap states near a vacancy into a resonance. Also, in the presence of the asymmetry, extended defects can lead to self-doping.[2–4]

Theoretical estimates of the value of t' vary.[5–7] Detailed calculations suggest that t' depends on interaction effects.[6] Experimentally, the parameter has been studied by using polarization-resolved magnetospectroscopy that reveals a difference in the energy separation between Landau levels for electron and hole bands. The first such experiment[8] performed several years ago inferred $t' \approx 0.9$ eV, but this high value could not be justified theoretically. However, the early devices were of low quality (graphene on silicon oxide with carrier mobility $\approx 10\,000$ cm^2 V^{-1} s^{-1}). The recent experiment[9] in high magnetic fields of ~ 20 T and using high-quality graphene

on graphite has found $|t'| \approx 0.4$ eV, which is consistent with theories, but still lies on the high side of the expected range.

I. QUANTUM CAPACITANCE MEASUREMENTS AND DETERMINATION OF t'

In this paper, to determine t', we have employed capacitance measurements of graphene encapsulated in hexagonal boron nitride (hBN). Our devices are schematically shown in the inset of Fig. 1. They are designed similarly to the graphene capacitors reported in Ref. 9 but exhibit higher quality and homogeneity, which are essential for the measurements' accuracy. Briefly, graphene is deposited on top of atomically flat hBN, and then another hBN crystal of a small thickness (15–25 nm) is deposited on top. An evaporated gold film completes the capacitor and serves as one of its electrode. The second electrode is graphene. The differential capacitance C of such devices is measured as a function of voltage bias V between the two electrodes by using a capacitance bridge.[10] C exhibits a typical value of 0.1–0.3 pF for our devices with an active area $S \approx 100$–200 μm^2. Measurements in magnetic fields reveal the onset of Landau quantization at ≈ 0.1 T, which yields a quantum mobility of $\approx 100\,000$ cm^2 V^{-1} s^{-1}. Comparison of this value with quantum mobility measured on similar encapsulated devices, but with smaller $S \approx 10$ μm^2, indicates that quantum oscillations in large graphene capacitors underestimate their mobility by a factor of a few. The disagreement can be explained because quantum oscillations are smeared not only by scattering but also by charge inhomogeneity that increases with increasing S.

The measured C consists of geometrical and quantum capacitance contributions.[10,11] The former capacitance C_G is independent on V and can be subtracted as a single fitting parameter that has a value close to the saturation value
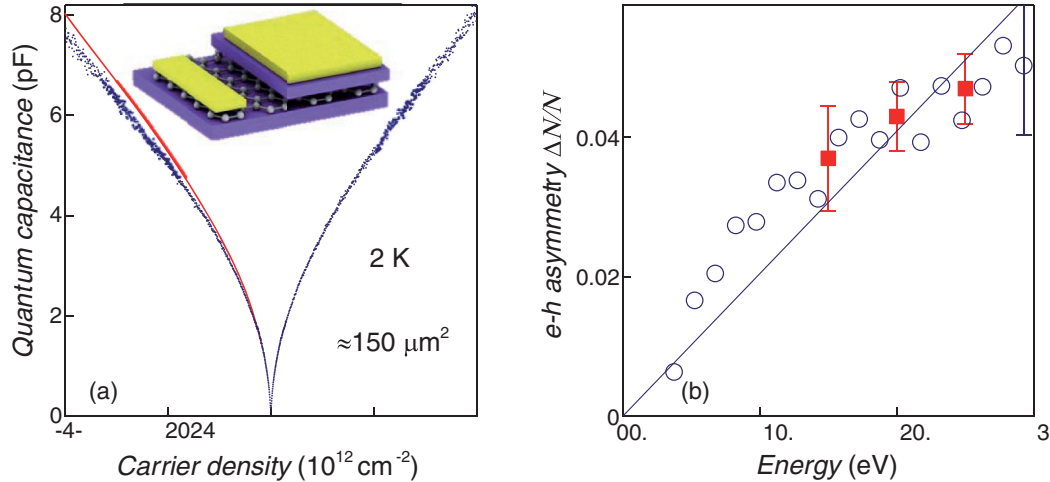
FIG. 1. (Color online) Asymmetry in the DoS of monolayer graphene. (a) Quantum capacitance as a function of n (positive and negative n refer to electrons and holes, respectively). Dots are the experimental data. The red curve mirrors the average behavior of C_Q at positive n to highlights the e-h asymmetry. Inset: devices' schematic. The top electrode and the gold contact to graphene are shown in yellow; hBN is in violet. (b) Asymmetry in the DoS. Blue circles are the experimental data averaged over consecutive energy intervals of 30 meV for the device in (a). The blue line is the best linear fit. Three red dots are measurements for four similar devices averaged over 100 meV and averaged over those devices. The bars show statistical errors. Our experimental accuracy is found to be highest around $\epsilon = 0.2$ eV because the asymmetry decreases with decreasing ϵ, whereas the accuracy of measuring C_Q also decreases with increasing ϵ because the geometrical capacitance start dominating C at high n.

of $C(V)$ at high V.[9] The resulting quantum capacitance $C_Q = Se^2 dn/d\mu$ can then be replotted as a function of carrier concentration n rather than V, where e is the electron charge, μ the chemical potential, and, for noninteracting electrons, $\frac{dn}{d\mu} = N(\epsilon_F)$ is the density of states (DoS) at the Fermi energy. Let us emphasize that for graphene devices with a thin gate dielectric, the usual approximation $n \propto V$ is no longer valid because C becomes a function V and changes by a factor of 2 for our typical devices at liquid-helium temperature. To this end, we have determined n by numerically integrating the experimentally measured $C(V)$ over V. For further details about our experimental devices, procedures, and data analysis, we refer to the earlier reports.[10,11]

Figure 1(a) shows $C_Q(n)$ for one of our devices. The quantum capacitance varies as $4Se^2\sqrt{|n|}/hv_F$, that is, approximately $\propto |\epsilon_F|$ (h is Planck's constant), yielding the Fermi velocity $v_F(n)$ of about 1×10^6 m/s. For $|n|$ below a few 10^{11} cm^{-2}, v_F shows a pronounced peak, increasing by a factor of 2, in good agreement with the previous measurements of many-body renormalization of the Dirac spectrum.[10,12] In this paper, we focus on e-h asymmetry, which is practically indiscernible within our experimental accuracy in the previously studied regime of low n but becomes notable at higher n. The red curve in Fig. 1(a) emphasizes this asymmetry. It is clear that the DoS for electrons N^+ is notably higher than that for holes N^-, and the difference increases with n. Figure 1(b) plots this difference $\Delta N = N^+ - N^-$, normalized to the average DoS, $\langle N \rangle = (N^+ + N^-)/2$. It is instructive to present ΔN as a function of the electron and hole energy ϵ rather than n. In the first approximation, ϵ can be calculated as $\epsilon_F = \hbar v_F \sqrt{n|/\pi}$, which assumes a constant v_F. We can also avoid this assumption by using the expression $\epsilon_F = eV - e^2 n S/C_G$.[9] Both approaches yield behavior that is practically indistinguishable over our range of n and presented in Fig. 1(b). It shows that, within

the experimental error, five capacitor devices studied in our paper exhibit the same values of ΔN, proving reliability of the results.

One can also see that the data in Fig. 1(b) can be fit by the linear dependence $\Delta N/N = \alpha \times \epsilon$ expected theoretically (see below). According to the tight-binding model, α is given by $\approx 6t'/t^2$. If we assume $t \approx 3$ eV, Fig. 1(b) yields $|t'/t| \approx 0.1$ or $t' \approx -0.3$ eV, with statistical accuracy of $\pm 10\%$. However, t itself has not been accurately defined ($|t| \approx 2.7$ eV has also been suggested in the literature), and this reduces the accuracy of determining t' to $\pm 15\%$. This value is three times lower than t' suggested in the early graphene work[8] and somewhat lower than ≈ 0.4 eV reported recently[8] (no accuracy was specified in the latter work).

A. General features of the bands near the Dirac point

The symmetry of the Brillouin zone of the honeycomb lattice severely constrains the form of the dispersion relation of the graphene π band near the K and K' points. In the following, we neglect the spin-orbit coupling. Then, the band dispersion at long wavelengths is isotropic and contains a linear and a quadratic contribution

$$\epsilon_k \approx \epsilon_0 \pm a|k| + bk^2 + \cdots \quad (2)$$

This dispersion can be identified term by term with the tight-binding expansion in Eq. (1). The periodicity of the π bands also implies that a set of localized Wannier functions can be defined, from which the dispersion relation in Eq. (2) can be extracted using effective tight-binding parameters. If the π bands do not overlap with other bands with the same symmetries, the Wannier functions are exponentially localized, and the tight-binding parameters decay with the distance between sites. Hence, one can rigorously identify the

parameters in Eq. (2) with effective tight-binding parameters, although they do not need be directly related to the atomic p_z orbitals. As far as the low energy, long wavelength properties are concerned, an effective tight-binding model contains the same information as a band Hamiltonian with the dispersion in Eq. (2).

In an interacting system, the quasiparticles near the chemical potential are still well defined, and their dispersion relation is given by Eq. (2). The effect of the interactions can be included into a self-energy correction. The self-energy for graphene must be consistent with Eq. (2), except for logarithmic corrections (see the following).

The self-energy of an interacting system also has an imaginary part, which describes the finite lifetime of quasiparticles away from the chemical potential. In principle, quasiparticles are no longer well defined at energies sufficiently far from the chemical potential, and interaction effects can prevent a precise definition of Wannier functions, which require a knowledge of the π bands at high energies. Even if this is the case, the equivalence between Eqs. (1) and (2) implies that the bands of graphene near the Dirac energy can be described by a tight-binding model.

Hence, when interactions are taken into account, a tight-binding description of the electronic Hamiltonian of graphene can be considered an effective model, which approximates accurately the properties of the system at low energies and long wavelengths. The range of validity of the model is of the order of the bandwidth of the π band, that is, a few electron volts.

B. Effect of interactions on e-h symmetry

The long-range part of the Coulomb interaction modifies the quasiparticle dispersion near the Dirac energy.[12,13] This effect can be formulated as the generation by the interaction of a self-energy, which has a contribution that depends logarithmically on the ratio between the high momentum cutoff of the model and the quasiparticle momentum[13]

$$\delta\epsilon_k \approx \delta_1\epsilon_k + \delta_2\epsilon_k + \cdots$$
$$\approx \pm\frac{e^2}{4\epsilon_0}k\log\left(\frac{\Lambda}{k}\right) + O\left(\frac{k^2}{\Lambda}\right) + \cdots \quad (3)$$

where k is the momentum, $\Lambda \approx a^{-1}$ the high k cutoff in the model, ϵ_0 the dielectric constant of the environment, and the signs in the first term refer to the conduction and valence bands. A k-independent constant, proportional to $e^2\Lambda/\epsilon_0$, has been omitted in Eq. (3). In renormalization group language, the terms left out in Eq. (2) are irrelevant, and they can be neglected in the limit $k/\Lambda \to 0$. In a condensed matter model, however, the ratio k/Λ is typically finite, and irrelevant terms give a finite, nonsingular contribution. If we describe the interactions in terms of the bare Coulomb potential, $v_q = (2\pi e^2)/(\epsilon_0 q)$ and estimate the self-energy by using the first-order perturbation theory, on dimensional grounds, we obtain[12]

$$\delta_2\epsilon_k = c\frac{e^2 k^2}{\epsilon_0\Lambda} \approx \bar{t}(ka)^2, \quad (4)$$

as the only available parameters are e^2/ϵ_0, Λ, and k. In Eq. (4) c is a numerical coefficient, and $\bar{t}$ is a parameter with dimension of energy.

Alternatively, we can use the Hartree-Fock approximation to estimate the self-energy. By using the Coulomb potential described previously and the wave functions derived from the Dirac approximation to the electronic bands, the self-energy can be written as[14]

$$\delta\epsilon_k^{HF} = -\frac{e^2}{4\pi\epsilon_0}\int_0^\Lambda k'dk'\int_0^{2\pi}d\theta\frac{1 \pm \cos\theta}{\sqrt{k^2 + k'^2 - 2kk'\cos\theta}},$$
$$(5)$$

where the two signs in the integral correspond to the valence and conduction bands. This expression can be expanded in powers of Λ:

$$\delta\epsilon_k^{HF} \approx -\frac{e^2\Lambda}{2\epsilon_0} \pm \frac{e^2}{4\epsilon_0}k\log\left(\frac{\Lambda}{k}\right) - \frac{e^2 k^2}{8\pi\epsilon_0\Lambda} + \cdots \quad (6)$$

The leading k-dependent term gives the logarithmic correction to the self-energy as per Eq. (3), whereas the next term has the same form as Eq. (3).

Both approaches mentioned previously suggest that a self-energy term, which depends quadratically on momentum k, can arise from electron-electron interactions, namely, from high-k exchange processes. It is determined by the short-range features of the interaction and the continuum approach used previously, that this cannot be expected to be numerically accurate. Unlike the logarithmic correction to the Fermi velocity, this term is not affected by the screening properties of the environment. Using the above formulas, we can estimate an effective next-nearest-neighbor hopping term t' as $\approx e^2/(18\epsilon_0\Lambda a^2)$. For $e^2/v_F \approx 2$ and $\epsilon_0 \approx 2$, we obtain $t' \approx -|t|/12$. This estimate is close to the value of t' found experimentally.

C. Influence of a large t' on graphene's properties

1. Defect states near the neutrality point

In neutral graphene, there can exist localized states that appear due to defects such as edges,[15–19] vacancies,[3] and other confinement effects.[4,20] For $t' = 0$, the wave functions associated with these states are finite only on one of the graphene sublattices; therefore, the states appear exactly at zero energy. These wave functions are also solutions of the local tight-binding equations when $t' \neq 0$ (see Appendix A). However, a finite value of t' modifies the boundary conditions and shifts the localized states from the Dirac point so that they become resonances with a finite decay width.

For the case of a vacancy, its state is shifted from zero energy ε by a value of the order of $\Delta\varepsilon \propto 3t'/[\log(R/a)]^{3/2}$, where R is a long-distance cutoff comparable to the size of a graphene device (see Appendix A). In practice, charge accumulation at the sites nearest to the vacancy shifts the resonance back to zero ε, so the site graphene remains neutral away from the vacancy. The smallness of the shift induced by t' is consistent with the experimental observation of sharp vacancy resonances.[21]

For a generic graphene edge of length L, which also gives rise to localized states, we expect that their number is a fraction of L/a, and their decay lengths range between L and a. Therefore, $\Delta\varepsilon$ due to a finite value of t' should vary between $t'(a/L)$ and t'. The additional DoS associated with graphene edges then changes from a delta function at zero ε to

$D(\varepsilon) \sim (L/a)/t'$ within the energy interval $0 \leqslant \varepsilon \leqslant t'$. The resonant states at vacancy or edge sites result in uncompensated spins, which should also exhibit e-h asymmetry. To compensate the spins requires a shift of the chemical potential of at least $\sim t'$, in agreement with the recent experiment.[22]

Self-doping at the edges is expected to result in charge accumulation,[2] which reduces the tendency towards the formation of uncompensated spins.[4,19]

2. Thermal self-doping

At a finite temperature T, the broken e-h symmetry due to t' induces different amounts of electrons and holes and, therefore, induces some doping at finite temperatures. The DoS is given by

$$D(\epsilon) \approx \frac{8\epsilon}{9\pi t^2 a^2} - \frac{8t'\epsilon^2}{3\pi t^3 a^2} + \cdots \qquad (7)$$

and, after some algebra, one can find the thermally induced DoS

$$n(T) \approx \frac{8Z(3)t'}{\pi t^4 a^2}(k_B T)^3 \approx 3.06\frac{t'(k_B T)^3}{t^4 a^2}, \qquad (8)$$

where $Z(3)$ is Riemann's Zeta function. For $T = 300$ K, we expect thermally induced electron doping at a level of $\approx 1.2 \times 10^9$ cm^{-2}, which can probably be observed in dedicated experiments.

3. Changes in Landau level structure

In low magnetic fields, where a continuum model is valid, the correction to the wave functions of the Landau levels in monolayer graphene induced by t' can be calculated analytically; see Appendix B. Their energies are shifted by a term proportional to the magnetic field

$$\epsilon_n \approx \begin{cases} \dfrac{9a^2 t'}{4\ell_B^2} & n = 0 \\[2mm] \dfrac{9a^2 t'}{2\ell_B^2}n \pm \sqrt{\dfrac{2nv_F^2}{\ell_B^2} + \left(\dfrac{9a^2 t'}{4\ell_B^2}\right)^2} & n \neq 0 \end{cases}, \qquad (9)$$

where $\ell_B^{-1} = \sqrt{|eB|/\hbar}$ is the magnetic length (see Refs. 8 and 23). The energies ϵ_n are measured with respect to the energy of the Dirac point. Note that the energy of the $n = 0$ Landau level acquires a dependence on the magnetic field. This state is localized in a single sublattice, as for $t' = 0$.

The situation is more complicated in bilayer graphene, where the low-energy spectrum consists of four inequivalent Dirac points within each valley, which appear due to trigonal warping. At zero interlayer bias and very low B such that $\ell_B \gg a(t^2/t_\perp t_3)$, numerous Landau levels emerge from this set of Dirac cones, where $t_\perp \approx 0.4$ eV is the interlayer hopping and t_3 gives the magnitude of trigonal warping.[24] There is one isotropic Dirac cone at $k = 0$ and three anisotropic cones at $k = 2t_\perp t_3/(3t^2 a)$. In the absence of next-nearest-neighbor hopping, the four Dirac cones lead to eight $n = 0$ Landau levels per valley. A finite value of t' changes the degeneracy of the four Dirac points into a singlet and a triplet. The energy difference between them is $t'(t_\perp t_3/t^2)^2$. The Fermi velocity of the bilayer Dirac cones is of the order of $t'a$; therefore, the energy splitting induced by t' can be resolved
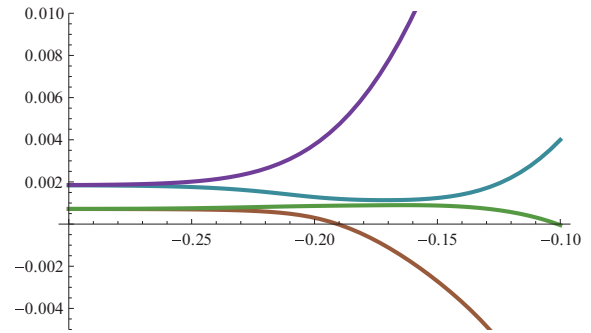

FIG. 2. (Color online) Dispersion of edge states for zero Landau level in bilayer graphene. $B = 25$ T; $t' = 0.4$ eV. The momentum of the state has been converted into the position of the guiding center.

if $\ell_B \gg a(t^2 t'/t_\perp t_3^2)^2$. For realistic parameters, this regime is reached in B of the order of a few millitesla.

On the other hand, the trigonal warping can be neglected at sufficiently high magnetic fields, $\ell_B \ll a(t^2/t_\perp t_3)$. In this case, there appears an eightfold degenerate Landau level near zero energy.[24,25] The degenerate set involves wave functions that correspond to the $n = 1$ Landau level of the electron gas, and a finite t' shifts their energy so that the eight levels are split into two quadruplets. The energy difference between the two subsets, to the lowest order in t' or B, is

$$\Delta\epsilon_0 \approx \frac{81t't^2 a^2}{8t_\perp^2 \ell_B^4}. \qquad (10)$$

This effect increases as B^2. The splitting of the bulk Landau levels gives an avoided crossing at the edge of a sample, as shown in Fig. 2.

The splitting between $n = 0$ Landau levels induced by t' is, however, much smaller than the splitting induced by electron-electron interactions. The latter is of the order of $e^2/(\epsilon_0 \ell_B)$.[26–30]

4. Influence of e-h asymmetry on Klein tunneling

The next-nearest-neighbor term t' changes the boundary conditions at interfaces, and the transmission through a ballistic *p-n* junction at the normal incidence becomes less than unity.[31] In a continuum model, the matching conditions at the *p-n* junction require the presence of evanescent waves with an inverse decay length $\lambda \approx t/(t'a) \approx 10a^{-1}$. This estimate implies that calculations of Klein tunneling in the presence of t' require numerical calculations using a discrete model.

The full calculation shown in Fig. 3 necessitates the inclusion of two evanescent waves in the classical forbidden region, a situation reminiscent of Klein tunneling through *p-n* junctions in bilayer graphene.[31,32] One can see that the effect of a finite t' is relatively small for realistic values of t' and even in the case of high barriers. The new evanescent waves have decay lengths much shorter than the lattice spacing and cannot induce major changes, either in the abrupt[31] or adiabatic[33] barrier limit.

5. Optical absorption in the presence of e-h asymmetry

Light absorption is determined by optical conductivity of graphene, which depends on the velocity-velocity correlations
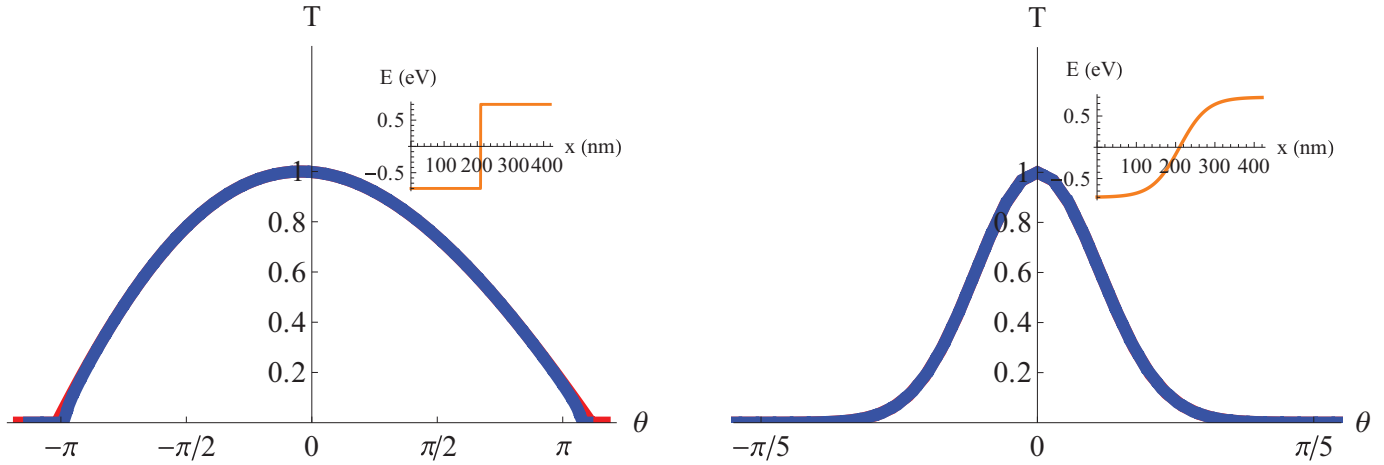
FIG. 3. (Color online) Transmission through a *p-n* junction in monolayer graphene as a function of incident angle. The chemical potentials on the left and right sides are -0.8 and 0.8 eV (see the insets). The red and blue (dashed) curves correspond to $t' = 0.01$ eV (effectively, zero t') and $t' = 0.3$ eV. Left: abrupt barrier with a width of 2 Å. Right: smooth, 100-nm-wide barrier. The barrier shapes used in the modeling are shown in the insets.

at finite frequencies and small wave vectors k.[34] A finite t' modifies the velocity operator that in the continuum limit becomes

$$\hat{v}_F(\vec{k}) \equiv v_F \vec{\sigma} + \frac{9t'a^2}{2} \vec{k} \begin{pmatrix} 1 & 0 \\ 0 & 1 \end{pmatrix}, \qquad (11)$$

where the velocity is expressed as an operator in the sublattice basis. The conductivity for $\vec{k} \to 0$ becomes

$$\sigma = \frac{e^2}{h} \frac{2}{\pi} \frac{v_F^2}{\omega} \int k\,dk\,\delta\big(\omega - \epsilon_k^c + \epsilon_k^v\big)$$
$$= \frac{e^2}{h} \frac{2}{\pi} \frac{v_F^2}{\omega} \int k\,dk\,\delta(\omega - 2v_F k) = \frac{e^2}{\hbar}, \qquad (12)$$

where ϵ_k^c and ϵ_k^v refer to the conduction and valence band. The contribution from t' to each quasiparticle energy vanishes when the difference is computed in Eq. (12); therefore, t' does *not* induce any change in the optical conductivity at any frequency for the asymmetric conical spectrum. This result explains the excellent agreement between the experimentally found $\sigma \approx \frac{e^2}{\hbar}$ at visible frequencies and the simple theory that did not take into account the e-h asymmetry.[35] Similarly, t' does not change the energy difference between the saddle

points of the p_z bands located at the M points of the Brillouin zone, although optical transitions between these states can be influenced by interactions within the e-h pair created by the photon.[36,37]

6. Plasmons

Changes in the Fermi velocity due to t' lead to changes in the plasmon dispersion described by

$$h\omega_p(q) = \sqrt{\frac{2e^2 h v_F(k_F)k_F q}{\epsilon_0}}, \qquad (13)$$

where $v_F(k_F) \approx 3ta/(2h) \pm 9t'a^2 k_F/(2h)$ and the different signs correspond to electrons and holes. Accordingly, the dependence of ω_p on n changes, and the plasmon frequencies become somewhat different for electrons and holes at the same density n.

7. Electronic susceptibility, magnetic impurities, and Ruderman-Kittel-Kasuya-Yosida interactions

For brevity, we consider here charge and spin susceptibilities at the neutrality point. For $t' \neq 0$, the charge susceptibility is

$$\chi_\rho(q) = \frac{q}{\pi^2 v_F} \int_0^{2\pi} d\theta \int_0^{\Lambda/q} \left(1 - \frac{k^2 - 1/4}{\sqrt{(k^2 + 1/4)^2 - k^2 \cos\theta^2}}\right)$$
$$\times \frac{k\,dk}{\sqrt{k^2 + 1/4 + k\cos\theta} + \sqrt{k^2 + 1/4 - k\cos\theta} + (9t'a^2 kq\cos\theta)/(4v_F)}. \qquad (14)$$

For $t' = 0$, this expression gives $\chi_\rho(q) = q/(4v_F)$. From Eq. (13), it is clear that the deviations induced by t' become important for $q \gtrsim v_F/t'a^2$, which is larger than Λ. A numerical integration of Eq. (14), setting $\Lambda = \infty$, is shown in Fig. 4.

The Ruderman-Kittel-Kasuya-Yosida (RKKY) interactions between fixed magnetic moments at different sites in the graphene lattice can be obtained from the Fourier transform of the charge susceptibility.[38,39] The factor in parenthesis
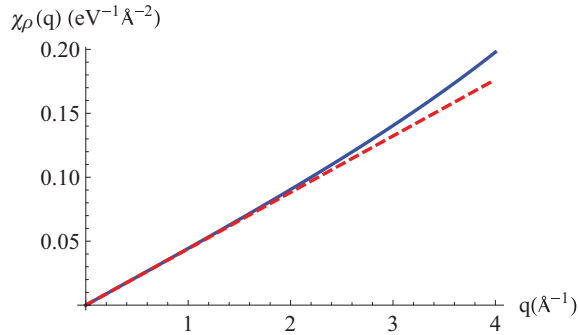
FIG. 4. (Color online) Static charge susceptibility of graphene for $t' = 0$ (red, dashed) and for $t' = 0.4$ eV (blue, full).

in Eq. (1) has to be replaced by 1 for the interaction between moments at sites in the same sublattice, and by $-(k^2 - 1/4)/\sqrt{(k^2 + 1/4)^2 - k^2 \cos\theta^2}$ for sites in different sublattices. As for $t' = 0$, the RKKY interaction is ferromagnetic for spins in the same sublattice and antiferromagnetic for sites in different sublattices. In both cases, the interaction decays as R^{-3}, where R is the distance between spins.

Finally, the formation of magnetic moments and the Kondo effect is sensitive to the hybridization between magnetic impurities and the graphene bands. This hybridization depends essentially on high-energy features of the band structure, such as the position of the van Hove singularities,[39] which are affected by the value of t'. As a result, the concentration dependence of the Kondo temperature should exhibit a strong e-h asymmetry, even for relatively small t', as follows from calculations for Co on graphene.[40]

8. Multilayer graphene

Bilayer and Bernal-stacked graphene exhibit parabolic bands at low energies with a dispersion relation $\epsilon_k \approx (hv_F k)^2/t_\perp$. The parameter t' induces another quadratic term in Eq. (1), however, which has a smaller magnitude. For the case of rhombohedral or ABC-stacked graphene, the simplest approximation gives a low-energy band with the dispersion relation $\epsilon_k \approx (hv_F k)^N/t_\perp^{N-1}$, where N is the number of layers.[41] The inclusion of the interlayer hopping term $\gamma_4 \approx 0.04$ eV modifies this dispersion,[42] which becomes, to the lowest order, $\epsilon_k \approx 3hv_F\gamma_4 ak^2/t_\perp$. For the found large $t' \approx 0.3$ eV, the contribution arising from Eq. (1) is comparable to the leading effect of interlayer coupling.

9. Effects of strain on next-nearest-neighbor hopping

Lattice deformations modify the tight-binding parameters and the hybridization between orbitals, leading to changes in the electronic structure.[43] The t' term leads to the appearance of a scalar potential if the graphene layer is curved.[44] In-plane strains change the interatomic distances and can also modify the value of t'. As a result, a different scalar potential is induced

$$V(\vec{r}) = -3t'\beta'[u_{xx}(\vec{r}) + u_{yy}(\vec{r})], \tag{15}$$

where $\beta' = \frac{a'}{t'}\frac{\partial t'}{\partial a'}$, a' is the distance between next-nearest-neighbor atoms, and u_{ij} is the strain tensor. There is a significant uncertainty regarding the scalar potential induced by strains.[45–47] For $t < 0$, we find a prefactor in Eq. (13) of

approximately 4 eV, which is consistent with the calculations in Ref. 46.

10. Other effects of finite t'

When studying localization phenomena in graphene with different kinds of disorder, the chiral symmetry intimately related to the e-h symmetry leads to important consequences determining the choice of the universality class.[48] Even relatively weak violation of these symmetries may in principle lead to important consequences, especially in the regime of low conductivity, that is, in the vicinity of the neutrality point.[39] Furthermore, the e-h symmetry or its absence can be crucial for nonlinear optics phenomena in graphene such as second-harmonic generation in the presence of valley polarization.[49]

II. CONCLUSION

Capacitance measurements reported here yield the next-nearest-neighbor hopping in graphene $t' \approx -0.3$ eV, which is close to the upper bound of theoretical estimates.[50] The sign and value of t' are consistent with estimates for the contribution from electron-electron interactions to the quasiparticle self-energy, expanding beyond the lowest-order approximation.

The t' term breaks the symmetry between electrons and holes as seen directly in the measured DoS in graphene. However, this asymmetry leads to relatively weak effects in the optical properties of graphene, its electronic transport, and plasmonics. The effect of t' on other low-energy phenomena, such as spin transport, is also expected to be negligible. Nonetheless, the additional hopping can induce nontrivial self-doping effects. In particular, resonances near lattice defects become shifted from zero energy, giving rise to bands of quasilocalized states with an energy width of t'. The hopping term is also expected to modify strongly the band structure of graphene multilayers with rhombohedral stacking. The dependence of t' on lattice deformations is consistent with estimates for the changes in chemical potential induced by strain.

Finally, let us note that e-h symmetry breaking terms, similar to t' considered here, can be expected near secondary Dirac points induced by superlattices[51–53] and in artificially engineered Dirac systems.[54,55]

APPENDIX A

1. Structure of the wave function of localized states at the Dirac energy

In the absence of nearest-neighbor hopping, $t' = 0$, the localized states that might exist in graphene at the Dirac energy have amplitude in one sublattice only.
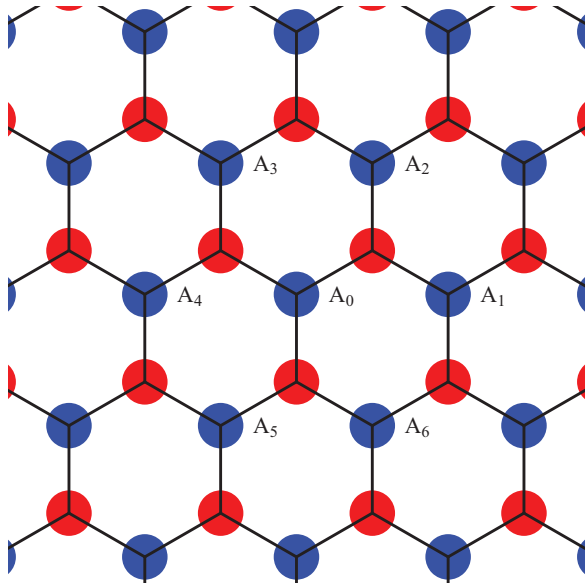
FIG. 5. (Color online) Notation used for the amplitudes of states at the Dirac energy.

FIG. 6. (Color online) Notation used for the amplitudes at the sites around a vacancy.

For $t' \neq 0$, localized states can still be defined at the Dirac energy, $\varepsilon_D = -3t'$, which are also defined in one sublattice only. Following the notation in Fig. 5, the amplitudes at the sites in the blue sublattice satisfy, for $t' = 0$,

$$
\begin{aligned}
t(A_0 + A_1 + A_2) &= 0, \\
t(A_0 + A_3 + A_4) &= 0, \\
t(A_0 + A_5 + A_6) &= 0,
\end{aligned}
\tag{A1}
$$

so

$$
t'(A_1 + A_2 + A_3 + A_4 + A_5 + A_6) = -3t' A_0, \tag{A2}
$$

which is the new tight-binding equation induced when $t' \neq 0$ and the energy is that of the Dirac point, $\varepsilon_D = -3t'$.

2. Resonance near a vacancy

Equation (A1) is not satisfied in the neighborhood of a vacancy. Instead, we obtain (see notations in Fig. 6):

$$
\begin{aligned}
A_1 = A_2 = A_3 &= \frac{A}{3} \\
A_1 + A_2 + A_3 &= A \neq 0,
\end{aligned}
\tag{A3}
$$

and, as a result,

$$
t'(B_1 + B_2 + B_3 + A_2 + A_3 + B_9) = 0. \tag{A4}
$$

This equation is the tight-binding equation associated with a shift of the energy at site A_1 by $\Delta\varepsilon_{A_1} = 9t'/A$. Similar equations can be written for sites A_2 and A_3. The constant A fixes the normalization of the wave function, $|A|^2 \propto 1/\log(R/a)$, where R is a long distance cutoff comparable to the dimensions of the graphene flake and a is a length of order of the interatomic distance.

The previous analysis shows that a quasilocalized state near a vacancy at the Dirac energy can be defined, for $t' \neq 0$, if the three sites around the vacancy are shifted by an energy $\Delta\varepsilon \propto 9t'/\sqrt{\log(R/a)}$, the case when $\Delta\varepsilon = 0$ can be seen as a weak perturbation. Then, for $\Delta\varepsilon = 0$, we expect a resonance
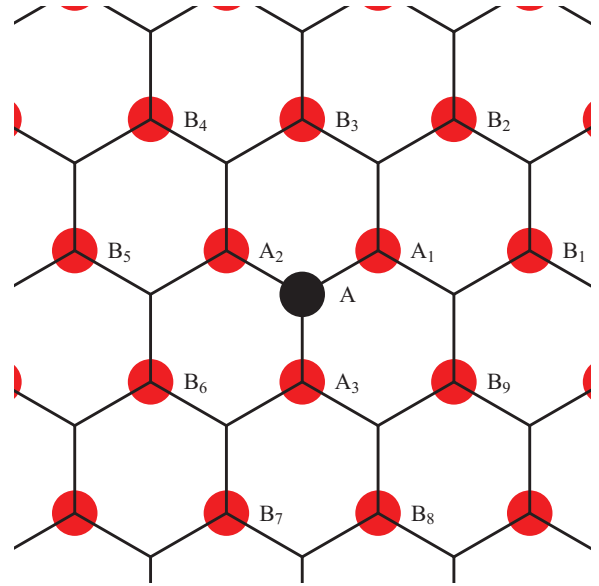
shifted from the Dirac energy by $\Delta\varepsilon \propto 3t'|A|^2/\sqrt{\log(R/a)} \propto 3t'/[\log(R/a)]^{3/2}$.

A similar analysis can be extended to localized states near a zigzag edge, and one obtains the results presented in Ref. 14.

APPENDIX B

1. Influence of t' on the Landau levels in monolayer graphene

In the continuum limit, we can use a basis of Landau levels defined in a given sublattice:

$$
\begin{aligned}
\Psi_{An} &\equiv \begin{pmatrix} |n\rangle \\ 0 \end{pmatrix} \\
\Psi_{Bn} &\equiv \begin{pmatrix} 0 \\ |n\rangle \end{pmatrix}.
\end{aligned}
\tag{B1}
$$

The Hamiltonian for a given corner of the Brillouin zone is

$$
H = \begin{pmatrix} \frac{9a^2 t'}{2\ell_B^2}\left(b^\dagger b + \frac{1}{2}\right) & \frac{\sqrt{2}v_F}{\ell_B} b \\ \frac{\sqrt{2}v_F}{\ell_B} b^\dagger & \frac{9a^2 t'}{2\ell_B^2}\left(b^\dagger b + \frac{1}{2}\right) \end{pmatrix}, \tag{B2}
$$

where $b^\dagger|n\rangle = \sqrt{n+1}|n+1\rangle$. The wave function for a given Landau level of energy ϵ_n and $n \neq 0$ can be written as

$$
\Psi_n \equiv \alpha_n \begin{pmatrix} |n-1\rangle \\ 0 \end{pmatrix} + \beta_n \begin{pmatrix} 0 \\ |n\rangle \end{pmatrix}, \tag{B3}
$$

with

$$
\begin{pmatrix} \frac{9a^2 t'}{2\ell_B^2}\left(n - \frac{1}{2}\right) & \frac{\sqrt{2}v_F}{\ell_B}\sqrt{n} \\ \frac{\sqrt{2}v_F}{\ell_B}\sqrt{n} & \frac{9a^2 t'}{2\ell_B^2}\left(n + \frac{1}{2}\right) \end{pmatrix} \begin{pmatrix} \alpha_n \\ \beta_n \end{pmatrix} = \epsilon_n \begin{pmatrix} \alpha_n \\ \beta_n \end{pmatrix}. \tag{B4}
$$

Expressions for ϵ_n are given in Eq. (8). Note that, for $t' = 0$ and $n \neq 0$, we have $\alpha_n = \pm\beta_n = \pm 1/\sqrt{2}$. The wave function for the Landau level with $n = 0$ is

$$
\Psi_0 \equiv \begin{pmatrix} 0 \\ |0\rangle \end{pmatrix}. \tag{B5}
$$

This expression is unchanged by t'. The velocity operator, needed for the calculation of the strength of optical transitions, becomes

$$\hat{v}_x \equiv v_F \begin{pmatrix} 0 & 1 \\ 1 & 0 \end{pmatrix} + \frac{9\sqrt{2}t'a^2}{2\hbar\ell_B} \begin{pmatrix} \frac{b^\dagger + b}{2} & 0 \\ 0 & \frac{b^\dagger + b}{2} \end{pmatrix}, \quad \text{(B6)}$$

$$\hat{v}_y \equiv v_F \begin{pmatrix} 0 & -i \\ i & 0 \end{pmatrix} + \frac{9\sqrt{2}t'a^2}{2\hbar\ell_B} \begin{pmatrix} \frac{b^\dagger - b}{2i} & 0 \\ 0 & \frac{b^\dagger - b}{2i} \end{pmatrix}. \quad \text{(B7)}$$

The strength of optical transitions between states n and $n\prime = \pm(n+1)$ is proportional to factors of order $|\pm v_F \alpha_n \beta_{n\prime}^* + \frac{9\sqrt{2}t'a^2}{2\hbar\ell_B}(\alpha_n \alpha_{n\prime}\sqrt{n'} \pm \beta_n \beta_{n\prime}\sqrt{n'+1})|^2$.

[1] A. H. Castro Neto, F. Guinea, N. M. R. Peres, K. S. Novoselov, and A. K. Geim, Rev. Mod. Phys. **81**, 109 (2009).

[2] N. M. R. Peres, F. Guinea, and A. H. Castro Neto, Phys. Rev. B **73**, 125411 (2006).

[3] V. M. Pereira, F. Guinea, J. M. B. Lopes dos Santos, N. M. R. Peres, and A. H. Castro Neto, Phys. Rev. Lett. **96**, 036801 (2006).

[4] M. Wimmer, A. R. Akhmerov, and F. Guinea, Phys. Rev. B **82**, 045409 (2010).

[5] S. Reich, J. Maultzsch, C. Thomsen, and P. Ordejón, Phys. Rev. B **66**, 035412 (2002).

[6] A. Grüneis, C. Attaccalite, L. Wirtz, H. Shiozawa, R. Saito, T. Pichler, and A. Rubio, Phys. Rev. B **78**, 205425 (2008).

[7] J. Jung and A. H. MacDonald, Phys. Rev. B **87**, 195450 (2013).

[8] R. S. Deacon, K. C. Chuang, R. J. Nicholas, K. S. Novoselov, and A. K. Geim, Phys. Rev. B **76**, 081406 (2007).

[9] M. Kühne, C. Faugeras, P. Kossacki, A. A. L. Nicolet, M. Orlita, Yu. I. Latyshev, and M. Potemski, Phys. Rev. B **85**, 195406 (2012).

[10] G. L. Yu, R. Jalil, Branson Belle, A. S. Mayorov, P. Blake, F. Schedin, S. V. Morozov, L. A. Ponomarenko, F. Chiappini, S. Wiedmann, U. Zeitler, M. I. Katsnelson, A. K. Geim, K. S. Novoselov, and D. C. Elias, Proc. Natl Acad. Sci. USA **110**, 3282 (2013).

[11] L. A. Ponomarenko, R. Yang, R. V. Gorbachev, P. Blake, A. S. Mayorov, K. S. Novoselov, M. I. Katsnelson, and A. K. Geim, Phys. Rev. Lett. **105**, 136801 (2010).

[12] D. C. Elias, R. V. Gorbachev, A. S. Mayorov, S. V. Morozov, A. A. Zhukov, P. Blake, K. S. Novoselov, A. K. Geim, and F. Guinea, Nat. Phys. **7**, 701 (2011).

[13] J. Gonzalez, F. Guinea, and M. A. H. Vozmediano, Nucl. Phys. B **424**, 595 (1994).

[14] N. M. R. Peres, F. Guinea, and A. H. Castro Neto, Phys. Rev. B **72**, 174406 (2005).

[15] K. Sasaki, S. Murakami, and R. Saito, Appl. Phys. Lett. **88**, 113110 (2006).

[16] M. Fujita, K. Wakayabashi, K. Nakada, and K. Kusakabe, J. Phys. Soc. Jpn. **65**, 1920 (1996).

[17] K. Nakada, M. Fujita, G. Dresselhaus, and M. S. Dresselhaus, Phys. Rev. B **54**, 17954 (1996).

[18] A. R. Akhmerov and C. W. J. Beenakker, Phys. Rev. B **77**, 085423 (2008).

[19] K. Harigaya, Chem. Phys. Lett. **340**, 123 (2001).

[20] M. I. Katsnelson and F. Guinea, Phys. Rev. B **78**, 075417 (2008).

[21] M. M. Ugeda, I. Brihuega, F. Guinea, and J. M. Gomez-Rodriguez, Phys. Rev. Lett. **104**, 096804 (2010).

[22] R. R. Nair, I-Ling Tsai, M. Sepioni, O. Lehtinen, J. Keinonen, A. V. Krasheninnikov, A. H. Castro Neto, M. I. Katsnelson, A. K. Geim, and I. V. Grigorieva, Nat. Commun. **4**, 2010 (2013).

[23] P. Plochocka, C. Faugeras, M. Orlita, M. L. Sadowski, G. Martinez, M. Potemski, M. O. Goerbig, J.-N. Fuchs, C. Berger, and W. A. de Heer, Phys. Rev. Lett. **100**, 087401 (2008).

[24] E. McCann and V. I. Fal'ko, Phys. Rev. Lett. **96**, 086805 (2006).

[25] K. S. Novoselov, E. McCann, S. V. Morozov, V. I. Fal'ko, M. I. Katsnelson, U. Zeitler, D. Jiang, F. Schedin, and A. K. Geim, Nat. Phys. **2**, 177 (2006).

[26] Y. Barlas, R. Côté, K. Nomura, and A. H. MacDonald, Phys. Rev. Lett. **101**, 097601 (2008).

[27] V. M. Apalkov and T. Chakraborty, Phys. Rev. Lett. **107**, 186803 (2011).

[28] M. Kharitonov, Phys. Rev. Lett. **109**, 046803 (2012).

[29] P. Maher, C. R. Dean, A. F. Young, T. Taniguchi, K. Watanabe, K. L. Shepard, J. Hone, and P. Kim, Nat. Phys. **9**, 154 (2013).

[30] D.-K. Ki, V. I. Fal'ko, and A. F. Morpurgo, arXiv:1305.4761.

[31] M. I. Katsnelson, K. S. Novoselov, and A. K. Geim, Nat. Phys. **2**, 620 (2006).

[32] R. Nandkishore and L. Levitov, Proc. Nat. Acad. Sci. USA **108**, 14021 (2011).

[33] V. V. Cheianov and V. I. Fal'ko, Phys. Rev. B **74**, 041403 (2006).

[34] N. M. R. Peres, Rev. Mod. Phys. **82**, 2673 (2010).

[35] R. R. Nair, P. Blake, A. N. Grigorenko, K. S. Novoselov, T. J. Booth, T. Stauber, N. M. R. Peres, and A. K. Geim, Science **320**, 1308 (2008).

[36] L. Yang, J. Deslippe, C.-H. Park, M. L. Cohen, and S. G. Louie, Phys. Rev. Lett. **103**, 186802 (2009).

[37] V. G. Kravets, A. N. Grigorenko, R. R. Nair, P. Blake, S. Anissimova, K. S. Novoselov, and A. K. Geim, Phys. Rev. B **81**, 155413 (2010).

[38] L. Brey, H. A. Fertig, and S. Das Sarma, Phys. Rev. Lett. **99**, 116802 (2007).

[39] M. I. Katsnelson, *Graphene: Carbon in Two Dimensions* (Cambridge University Press, Cambridge, UK, 2012).

[40] T. O. Wehling, A. V. Balatsky, M. I. Katsnelson, A. I. Lichtenstein, and A. Rosch, Phys. Rev. B **81**, 115427 (2010).

[41] F. Guinea, A. H. Castro Neto, and N. M. R. Peres, Phys. Rev. B **73**, 245426 (2006).

[42] Mikito Koshino and Edward McCann, Phys. Rev. B **80**, 165409 (2009).

[43] M. A. H. Vozmediano, M. I. Katsnelson, and F. Guinea, Phys. Rep. **496**, 109 (2010).

[44] E. A. Kim and A. H. Castro Neto, Europhys. Lett. **84**, 57007 (2008).

[45] K. Sugihara, Phys. Rev. B **28**, 2157 (1983).

[46] H. Suzuura and T. Ando, Phys. Rev. B **65**, 235412 (2002).

[47] S.-M. Choi, S.-H. Jhi, and Y.-W. Son, Phys. Rev. B **81**, 081407 (2010).

[48] F. Evers and A. D. Mirlin, Rev. Mod. Phys. **80**, 1355 (2008).

[49] T. O. Wehling, A. Huber, A. I. Lichtenstein, and M. I. Katsnelson (unpublished).

[50] The sign of the nearest-neighbor hopping t does not have experimental consequences in a bipartite lattice. Comparisons between tight-binding models and local-density approximation calculations in C_{60}, which does not have a bipartite lattice, suggests that in

sp^2-bonded carbon compounds $t < 0$; see E. Manousakis, Phys. Rev. B **44**, 10991 (1991).

[51] L. A. Ponomarenko, R. V. Gorbachev, G. L. Yu, D. C. Elias, R. Jalil, A. A. Patel, A. Mishchenko, A. S. Mayorov, C. R. Woods, J. R. Wallbank, M. Mucha-Kruczynski, B. A. Piot, M. Potemski, I. V. Grigorieva, K. S. Novoselov, F. Guinea, V. I. Fal'ko, and A. K. Geim, Nature (London) **497**, 594 (2013).

[52] C. R. Dean, L. Wang, P. Maher, C. Forsythe, F. Ghahari, Y. Gao, J. Katoch, M. Ishigami, P. Moon, M. Koshino, T. Taniguchi, K. Watanabe, K. L. Shepard, J. Hone, and P. Kim, Nature (London) **497**, 598 (2013).

[53] B. Hunt, J. D. Sanchez-Yamagishi, A. F. Young, M. Yankowitz, B. J. LeRoy, K. Watanabe, T. Taniguchi, P. Moon, M. Koshino, P. Jarillo-Herrero, and R. C. Ashoori, Science **340**, 1427 (2013).

[54] K. K. Gomes, W. Mar, W. Ko, F. Guinea, and H. C. Manaharan, Nature (London) **483**, 306 (2012).

[55] M. Polini, F. Guinea, M. Lewenstein, H. C. Manoharan, and V. Pellegrini, Nat. Nanotechnol. **8**, 625 (2013).